ACS APPLIED MATERIALS & INTERFACES

RESEARCH ARTICLE

www.acsami.org

Diketopyrrolopyrrole-Based π-Bridged Donor−Acceptor Polymer for Photovoltaic Applications

Wenting Li,[†] Taegweon Lee,[†] Soong Ju Oh,[‡] and Cherie R. Kagan*[,†,‡,§]

[†]Department of Chemistry, [‡]Department of Materials Science and Engineering, and [§]Department of Electrical and Systems Engineering, University of Pennsylvania, Philadelphia, Pennsylvania 19104

Supporting Information

ABSTRACT: We report the synthesis, properties, and photovoltaic applications of a new conjugated copolymer (C12DPP-π-BT) containing a donor group (bithiophene) and an acceptor group (2,5-didodecylpyrrolo[3,4-c]pyrrole-1,4(2H,5H)-dione), bridged by a phenyl group. Using cyclic voltammetry, we found the energy levels of C12DPP-π-BT are intermediate to common electron donor and acceptor photovoltaic materials, poly (3-hexylthiophene-2,5-diyl) (P3HT) and [6,6]-phenyl-C61-butyric acid methyl ester (PCBM), respectively. Whereas P3HT and PCBM are exclusively electron donating or accepting, we predict C12DPP-π-BT may uniquely serve as either an electron donor or an acceptor when paired with PCBM or P3HT forming junctions with large built-in potentials. We confirmed the ambipolar nature of C12DPP-π-BT in space charge limited current measurements and in C12DPP-π-BT:PCBM and C12DPP-π-BT:P3HT bulk heterojunction solar cells, achieving power conversion efficiencies of 1.67% and 0.84%, respectively, under illumination of AM 1.5G (100 mW/cm^2). Adding diiodooctane to C12DPP-π-BT:PCBM improved donor−acceptor inter-mixing and film uniformity, and therefore enhanced charge separation and overall device efficiency. Using higher-molecular-weight polymer C12DPP-π-BT in both C12DPP-π-BT:PCBM and C12DPP-π-BT:P3HT devices improved charge transport and hence the performance of the solar cells. In addition, we compared the structural and electronic properties of C12DPP-π-BT:PCBM and C12DPP-π-BT:P3HT blends, representing the materials classes of polymer:fullerene and polymer:polymer blends. In C12DPP-π-BT:PCBM blends, higher short circuit currents were obtained, consistent with faster charge transfer and balanced electron and hole transport, but lower open circuit voltages may be reduced by trap-assisted recombination and interfacial recombination losses. In contrast, C12DPP-π-BT:P3HT blends exhibit higher open circuit voltage, but short circuit currents were limited by charge transfer between the polymers. In conclusion, C12DPP-π-BT is a promising material with intrinsic ambipolar characteristics for organic photovoltaics and may operate as either a donor or acceptor in the design of bulk heterojunction solar cells.

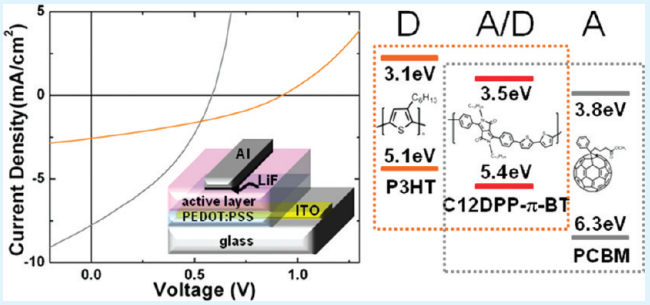

KEYWORDS: bulk heterojunction polymer solar cells, donor−acceptor, diketopyrrolopyrrole, PCBM, P3HT

1. INTRODUCTION

Organic photovoltaics (OPVs) continue to attract growing attention as candidates for the low-cost fabrication of relatively high efficiency solar cells, to make future solar technology competitive with traditional energy resources.[1−6] The most promising and popular strategy is the design of bulk heterojunction (BHJ) OPVs where an active layer comprises a composite of a donor and an acceptor material. The BHJ architecture requires the donor and acceptor materials to be tailored to provide (1) strong and broad absorption of solar radiation; (2) a staggered energy level structure to drive charge separation, yet have a large difference between the donor ionization energy and the acceptor electron affinity to maintain a large cell open circuit voltage; and (3) high hole and electron mobilities for facile charge collection. Here we adopted the strategy of designing a conjugated copolymer, which incorporates electron-rich donor and electron deficient acceptor segments, linked by a bridging unit in the polymer backbone. This structure provides an easy and efficient way to adjust the physical properties of the polymer by chemically modifying the donor, the acceptor and/or the linking group. Donor−acceptor copolymers are known for intrachain push−pull charge transfer, which has been used to synthesize more conjugated, lower band gap polymers having extended overlap with the solar spectrum.[7−9] However, materials with narrow bandgap sometimes suffer from low open circuit voltage (V_{oc}) arising from the reduction of the built-in potential between the highest occupied molecular orbital (HOMO) level of the donor and lowest unoccupied molecular orbital (LUMO) level of the acceptor. Fortunately, it is possible to adjust the aromaticity of the polymer, for instance, by adjusting the linking group, to balance polymer absorption and V_{oc} to optimize OPV performance.[10,11]

In this study, we have taken advantage of the recently developed diketopyrrolopyrrole (DPP)-based polymer and designed a new conjugated copolymer (C12DPP-π-BT) containing the donor

Received: June 3, 2011
Accepted: September 3, 2011
Published: September 03, 2011

group bithiophene (BT) and the acceptor group 2,5-didodecylpyrrolo-[3,4-c]pyrrole-1,4(2H,5H)-dione (C12DPP), bridged by a phenyl group (π). We chose electron rich bithiophene (BT) as the donor group because of its excellent electron donating ability and its electrochemical stability in PV devices.[12] For the choice of the acceptor group, the highly conjugated lactam planar structure of electron deficient diketopyrrolopyrrole (DPP) provides an idea building block, which results in strong $\pi-\pi$ interactions for efficient charge transport. The first diketopyrrolopyrrole based polymer was reported by Yu[13,14] and developed further by Tieke.[15−17] DPP has strong absorption in the visible and has been used as a donor material in the fabrication of BHJ OPVs in conjunction with PCBM.[1,9,10,18] Its relatively low lying HOMO and LUMO levels also make it a promising candidate as an acceptor material when blended with polymers possessing higher lying energy levels for application in hybrid solar cells.[19] To further optimize the energy levels, we chose a phenyl group instead of commonly used thiophene as the linking group to adjust the aromaticity to lower the HOMO level (to 5.4 eV) of the polymer. In addition, when the HOMO level lies well below the air oxidation threshold (5.27 eV), it improves air stability.[20] We also introduce a dodecyl side group to increase the solubility of the polymer in common solvent systems to allow solution processability.

To compare with the literature, in most reported work, DPP containing polymers are almost exclusively used as an electron donor in photovoltaics.[18,21−24] Janssen recently reported the application of DPP as acceptor materials in organic photovoltaics with the highest power conversion efficiency of 0.31%.[19] In comparison, by choosing the donor/acceptor pair and adjusting the linking group, the balanced conjugated structure of C12DPP-π-BT and the suitable HOMO/LUMO levels intermediate to the common electron donor (P3HT) and the electron acceptor (PCBM), make this polymer unique, so it may serve as either an electron donor or acceptor in blends with different semiconducting components, to form efficient OPV devices. A moderate power conversion efficiency of 1.67% was achieved with the C12DPP-π-BT used as the donor material by blending with PCBM and 0.84% with C12DPP-π-BT used as the acceptor material by blending with P3HT when deposited from chloroform.

2. EXPERIMENTAL SECTION

2.1. Synthesis. All experiments were performed under a nitrogen atmosphere by standard Schlenk techniques. THF was freshly distilled from sodium benzophenone under N_2 prior to use. After degassing with N_2 for 30 min, $Pd(PPh_3)_4$ (0.058 g, 0.05 mmol) was added to a stirred toluene solution (5 mL) of 3,6-bis(4-bromophenyl)-2,5-didodecylpyrrolo-[3,4-c]pyrrole-1,4-dione (**1**, C12DPP-π-Br_2) (0.39 g, 0.5 mmol) and 5,5′-bis(trimethylstannyl)-2,2′-bithiophene (**2**) (0.25 g, 0.5 mmol). The reaction mixture was heated at 100 °C for 2 days under nitrogen. The raw product was precipitated with methanol and collected by filtration. The precipitate was dissolved in chloroform and filtered with Florisil Adsorbent for Chromatography 60-100 mesh to remove the metal catalyst and inorganic impurities. The final product C12DPP-π-BT was obtained by precipitating in methanol and washing with hexanes. Yield: 86%. ^{1}H NMR ($CDCl_3$, 360 MHz): δ 0.86-0.88 (m, 6H, C−CH_3), 1.14−1.20 (m, 36H, C−CH_2), 1.58 (m, 4H, C−CH_2), 3.74 (m, 4H, N−CH_2), 6.98 (m, 2H, Th), 7.16 (m, 2H, Th), 7.40 (d, 4H, Ph), 7.62 (d, 4H, Ph). Gel permeation chromatographic (GPC) analysis: number-average molecular weight (M_n) = 5.88×10^3 g/mol, weight-average molecular weight (M_w) = 10.35×10^3 g/mol, and polydispersity index (PDI) = 1.76 (against polystyrene standard). A higher M_n polymer was prepared using the same procedure as described for low M_n C12DPP-π-BT, except that $Pd_2(dba)_3$/P(*o*-tolyl)$_3$ was used instead of the $Pd(PPh_3)_4$ catalyst. Yield: 82%. GPC analysis: M_n = 12.36×10^3 g/mol, M_w = 17.68×10^3 g/mol, and PDI = 1.43 (against polystyrene standards).

All chemicals were purchased from Aldrich, Alfa Aesar, TCI, and used without further purification. $Pd(PPh_3)_4$,[25] 5,5′-bis(trimethylstannyl)-2,2′-bithiophene,[26,27] and 3,6-Bis(4-bromophenyl)-2,5-didodecylpyrrolo [3,4-*c*]pyrrole-1,4-dione **1**[28] were prepared according to literature procedures.

2.2. Characterization. ^{1}H NMR spectra were recorded with a Bruker Avance (360 MHz) spectrometer. Molecular weights and polydispersity indices (PDIs) of the polymers were determined by gel permeation chromatography (GPC) analysis with a polystyrene standards calibration. Cyclic voltammograms were obtained employing a three electrode C3 cell stand and Epsilon electrochemical workstation (Bioanalytical Systems, Inc.). 0.01 M tetrabutylammonium hexafluorophosphate ($TBAPF_6$) was used as the supporting electrolyte in acetonitrile. A platinum disk and platinum wire were selected as working and counter electrodes, respectively. A $Ag/AgNO_3$ (non-aqueous) electrode was used as the reference electrode. The redox couple ferrocene/ferrocenium ion (Fc/Fc^+) provided an external standard.

Absorption and Photoluminescence (PL) spectra were measured as spin-coated films on quartz substrates, using a Varian Cary 5000 UV-Vis-NIR spectrophotometer and a Fluorolog 3 spectrofluorometer (HORIBA Jobin Yvon, Ltd., excitation at 550 nm), respectively. AFM (Atomic force microscopy) measurements were carried out using a Digital Instruments Multimode AFM operated in tapping mode. TEM (transmission electron microscopy) images were obtained using a JEM-1400 (JEOL Ltd.).

2.3. Fabrication and Characterization of Solar Cells. Polymer solar cells were fabricated on indium tin oxide (ITO) coated glass substrates (Delta Technologies, nominal coating thickness, 120-160 nm, sheet resistance, 5-15 Ω/sq). The ITO on glass was first patterned by photolithography, thoroughly cleaned by ultrasonication in acetone and isopropanol, rinsed with DI water, dried on a hot plate at 180°C for 30 min, and finally treated by UV-ozone for 30 min. A 40 nm film of poly(3,4-ethylenedioxythiophene)/poly(styrene sulfonate) was deposited on the ITO by spin-coating from an aqueous PEDOT:PSS dispersion (PEDOT:PSS, Baytron P VP AI4083) at 2000 rpm in air. The PEDOT:PSS film was dried at 180°C for 20 min inside the N_2 glovebox. Subsequent processing steps were carried out in the N_2 glovebox. Either a C12DPP-π-BT:PCBM mixture (15 mg/mL, weight ratio: 1:2) or a C12DPP-π-BT:P3HT (10 mg/mL, weight ratio: 1:1) mixture was dissolved in chlorofrom, and in some cases 5 wt % diiodooctane was added to the C12DPP-π-BT:PCBM mixture. The blend solution was deposited by spin-coating on top of the PEDOT:PSS layer at 1500 rpm for one minute and then annealed at 140 °C for 20 min. The devices were transferred into the vacuum evaporation chamber and kept there for three hours under vacuum (<1×10^{-6} Torr) prior to evaporating a back contact consisting of 1 nm LiF and 80 nm Al through shadow masks. The active device area of 9 mm^2 is defined by the overlapping area of the back LiF/Al contact and the front, lithographically pre-patterned, transparent, ITO contact.

Current−voltage characteristics of the photovoltaic cells were acquired using a Keithley 2400 source-meter under the illumination of AM 1.5G solar simulated light (1 sun, 100 mW/cm^2, Oriel instruments model 96000, Newport Co.) in air. A reference cell and meter (Model: 91150, Newport Co.) were used to calibrate the light intensity.

Spatially resolved measurements of solar cell short circuit current were collected for C12DPP-π-BT:PCBM (with and without the diiodooctane additive) and C12DPP-π-BT:P3HT devices. 488 nm light from an Innova 70C Spectrum Ar:Kr laser was focused to a spot size of 0.4 μm using a modified Olympus BH2 microscope to illuminate devices through the transparent ITO contact. Devices were mounted on

Scheme 1. Synthesis and Structure of C12DPP-π-BT[a]

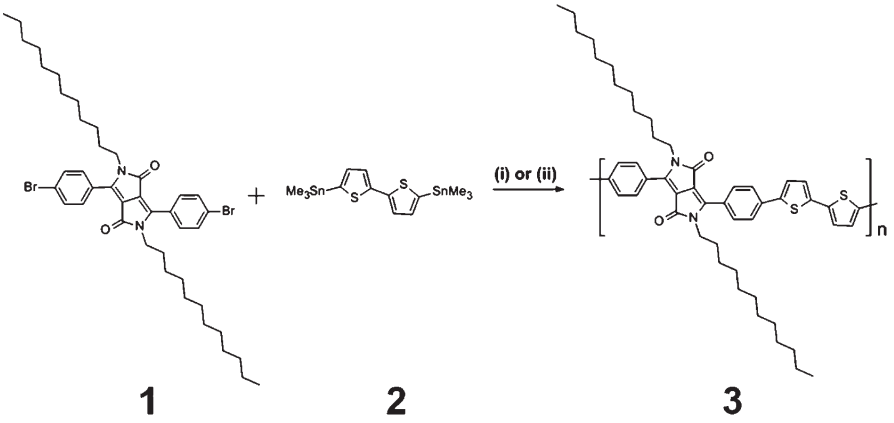

[a] (i) 0.05 mmol $Pd(PPh_3)_4$, toluene, 90 °C for low molecular weight. (ii) 0.05 mmol $Pd_2(dba)_3$, 0.4 equiv of P(o-tolyl)$_3$, toluene, 90 °C for high molecular weight.

a piezo−controlled stage (Max 301, Thor Labs Nanomax) for photocurrent mapping. Local photocurrent data were acquired in 0.25 μm steps across 10 μm by 10 μm devices areas.

2.4. Space Charge Limited Current (SCLC) Measurements. For hole mobility measurements, devices were fabricated on photolithographically patterned ITO coated glass substrates, cleaned and coated with a 40 nm PEDOT:PSS film. Films of C12DPP-π-BT or P3HT were deposited by spin-coating followed by annealing. The same fabrication procedures were used as described above for solar cell fabrication, except 60 nm Pd back contacts were evaporated through shadow masks to characterize hole transport by SCLC measurements.

For electron mobility measurements, devices were fabricated on 2.5 cm x 2.5 cm glass slides, using the same cleaning procedures as for solar cells. 20 nm Al back contacts and 1 nm LiF and 60 nm Al front contacts were deposited by thermal evaporation. Films of C12DPP-π-BT or PCBM were similarly explored. Samples for hole and electron mobility measurements were fabricated side-by-side for comparison.

2.5. Recombination Characterization by Photoconductivity Measurements. On pre-cleaned quartz disks, 5 μm channel length, 75 μm channel width junctions were photolithographically defined and 1 nm Cr/19 nm Au was thermally evaporated to form bottom-contact, two-terminal devices for photoconductivity measurements. Films of C12DPP-π-BT, C12DPP-π-BT:PCBM (5 wt % diiodooctane added) and C12DPP-π-BT:P3HT were deposited by spin-casting from chloroform solutions. The devices were annealed at 140 °C for 20 min.

Photoconductivity measurements were performed in ambient air. The devices were illuminated by 488 nm laser excitation from an Ar−Kr laser (Innova 70C Spectrum). Neutral-density filters were used to control excitation intensity. Bias voltage was applied and the photocurrent was recorded using a source-meter (Keithley model 2400).

3. RESULTS AND DISCUSSION

3.1. Synthesis. Scheme 1 illustrates the synthetic procedure for the conducting polymer C12DPP-π-BT (poly 3-(4-(2,2′-bithiophen-5-yl)phenyl)-2,5-didodecyl-6-phenylpyrrolo[3,4-c]pyrrole-1,4(2H,5H)-dione), containing electron deficient C12DPP (2,5-didodecylpyrrolo[3,4-c]pyrrole-1,4(2H,5H)-dione) and electron rich bithiophene monomers, bridged by a phenyl group. 3,6-Bis-(4-bromophenyl)-2,5-didodecylpyrrolo[3,4-*c*]pyrrole-1,4-dione (**1**, C12DPP-Br_2) was synthesized by a procedure similar to that of Tieke.[28] 5,5′-bis(trimethylstannyl)-2,2′-bithiophene (**2**) was reacted with 1 equivalent of **1** by Stille cross coupling in the presence of a catalytic amount of $Pd(PPh_3)_4$ in toluene to obtain C12DPP-π-BT. After work-up, a shiny light brown solid was acquired. GPC analysis indicates it has a M_n of 5.88×10^3g/mol, M_w of 10.35×10^3 g/mol, and PDI of 1.76. Based on previous reports, higher molecular weight conducting polymers are more favorable for the fabrication of efficient OPVs.[29] The catalyst system of $Pd_2(dba)_3$/P(*o*-tolyl)$_3$ was adopted and C12DPP-π-BT with double the molecular weight was yielded, having a high M_n of 12.36×10^3 g/mol, M_w of 17.68×10^3 g/mol, and PDI of 1.43. The low PDI of both polymers indicated a narrow distribution of individual molecular masses in these samples. Both polymers were readily soluble in common organic solvents such as toluene, chloroform, and chlorobenzene.

3.2. Energy Level Measurements Using the Cyclic Voltammetry Method. To achieve efficient charge separation and high conversion efficiency in a heterojuntion solar cell, we must stagger the energy levels of the two components, and the energy difference between the ionization energy of the donor and the electron affinity of the acceptor must drive charge transfer of the photogenerated excitation and provide a sufficient built-in potential to attain a high open circuit voltage (V_{oc}).[30−32] Electrochemical measurements were used to study the electronic structure of C12DPP-π-BT, and to characterize the alignment of its energy levels relative to common organic photovoltaic materials used in bulk heterojunction devices: the electron donor P3HT and the electron acceptor PCBM. Figure 1a−d shows cyclic voltammograms collected for drop cast films of (a) high and (b) low M_n C12DPP-π-BT, (c) PCBM, and (d) P3HT on a platinum working electrode. The values were recorded against the potential of ferrocene/ferrocenium (Fc/Fc^+) redox couple, which served as an external standard in our system. We adopted the commonly used scale of -4.8 eV[33] versus vacuum for Fc/Fc^+ to consistently derive the energy levels for all of the active components. A recent report by Bazan highlights inconsistencies in the scale for Fc/Fc^+ redox couple standard and the necessary approximation in correlating electrochemical potentials measured in solution with HOMO/LUMO energies scaled in vacuum, which lead to uncertainties in our knowledge of the absolute energy levels of the active materials.[34] We note all of the active materials reported here were measured under the same laboratory conditions, therefore the energy levels would be

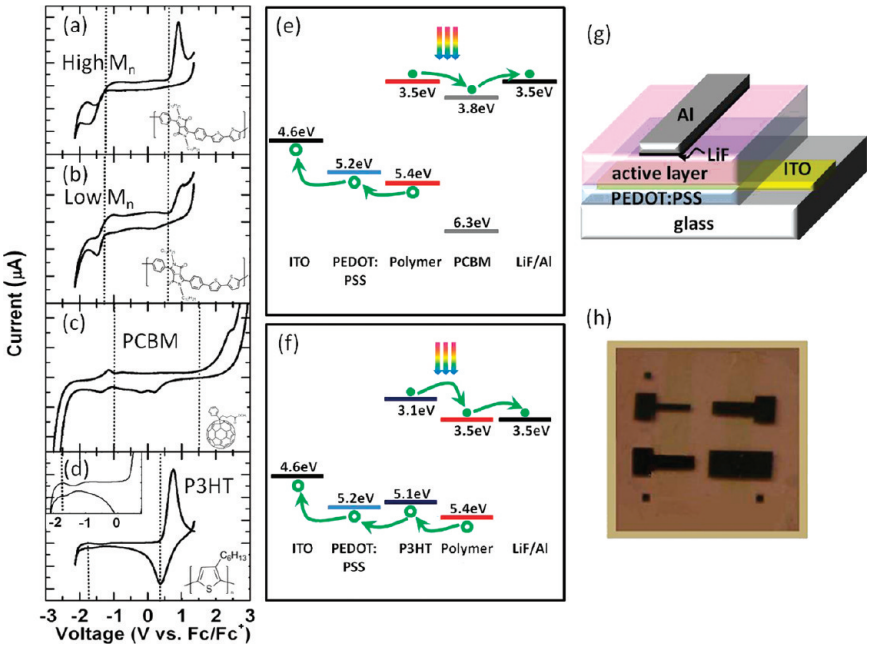

Figure 1. Cyclic voltammograms of (a) high M_n C12DPP-π-BT, (b) low M_n C12DPP-π-BT, (c) PCBM, and (d) P3HT films on a platinum working electrode in an acetonitrile solution of 0.01 M $TBAPF_6$ at a scan rate of 50 mV/s. Redox couple ferrocene/ferrocenium (Fc/Fc^+) was used as an external standard. (e, f) Energy level alignment of active layer components derived from cyclic voltammograms (assuming a Fc/Fc^+ scale of −4.8 eV) and electrode materials from literature reported values, in reference to vacuum. (g) Schematic and optical micrographs of polymer photovoltaic devices.

Table 1. Optical and Electrochemical Properties of the C12DPP-π-BT, P3HT, and PCBM

	UV−vis absorption				cyclic voltammetry		
	solution	film			p-doping	n-doping	
composites	λ_{max} (nm)	λ_{max} (nm)	λ_{onset} (nm)	E_g^{opt}(eV)	E_{on}^{ox}/HOMO (V)/(eV)	E_{on}^{red}/LUMO (V)/(eV)	E_g^{EC} (eV)
high M_n C12DPP-π-BT	557	580	690	1.80	0.6/−5.4	−1.3/−3.5	1.9
low M_n C12DPP-π-BT	548	580	690	1.80	0.6/−5.4	−1.3/−3.5	1.9
P3HT	450	525	650	1.91	0.3/−5.1	−1.7/−3.1	2.0
PCBM[a]					1.5/−6.3	−1.0/−3.8	2.5

[a] PCBM film has a broad absorption in the visible region (350−750 nm) without a distinguishable peak.

equally shifted if a different scale for Fc/Fc^+ were adopted. Both polymers show quasi-reversible oxidation peaks without significant changes after several cycles when swept negatively, and an irreversible reduction peak when swept positively. On the basis of the onset of the oxidation peak at 0.6 V and reduction peak at −1.3 V of both low and high M_n C12DPP-π-BT, we estimated the HOMO and LUMO levels of C12DPP-π-BT to be −5.4 and −3.5 eV, respectively. Similarly, from the cyclic voltammograms in Figure 1c,d, we estimated the HOMO/LUMO energy levels of PCBM and P3HT to be −6.3 eV/−3.8 eV and −5.1 eV/−3.1 eV, respectively. The HOMO/LUMO levels for PCBM and P3HT are in agreement with literature reported values.[35,36] The electrochemical bandgap, calculated from the difference between the HOMO and LUMO energies, is 1.9 eV for both the high and low M_n polymers. The electrochemical bandgaps are consistent with the optical band gaps of 1.8 eV for both polymers, calculated from the onset in optical absorptions, described in detail in the next section. The difference between the electrochemical bandgap and the optical bandgap reflects the measurement influences of solvents, ions, and surface effects present in electrochemical measurements and the optically excited excitonic state, stabilized by the Coulomb binding energy of the exciton in absorption spectroscopy.[37] The results are summarized in Table 1.

Figure 1e,f shows the schematic of the energy level diagram constructed from the reported work functions of electrode materials LiF/Al and ITO/PEDOT:PSS,[38−40] and the HOMO and LUMO energies derived from cyclic voltammograms for C12DPP-π-BT, PCBM, and P3HT. The HOMO and LUMO of C12DPP-π-BT are higher compared with those for PCBM, which is consistent with C12DPP-π-BT serving as an electron donor in C12DPP-π-BT:PCBM blends. In contrast, when blended with P3HT, the HOMO and LUMO of C12DPP-π-BT lie below those of P3HT, which is consistent with C12DPP-π-BT acting as an electron acceptor in C12DPP-π-BT:P3HT blends. As generally accepted, built-in potential is directly related to the maximum value of open circuit voltage, which can be estimated by the energy difference between the HOMO level of the donor and LUMO level of the acceptor (or equivalently the energy difference between the ionization potential of the donor and the electron affinity of the acceptor).[30] Compared with the

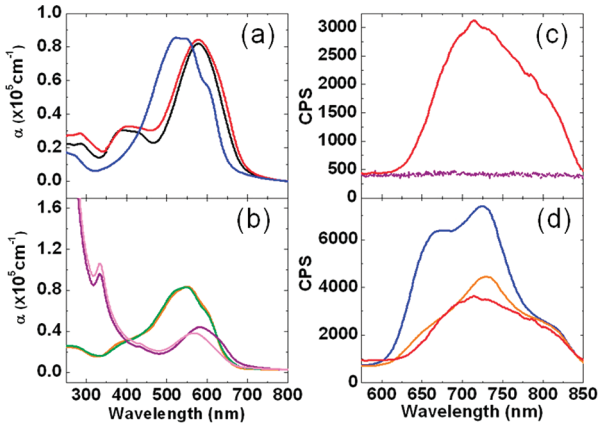

Figure 2. (a) UV−vis absorption spectra of high (red) and low (black) M_n C12DPP-π-BT and pristine P3HT (blue) in thin films. (b) UV−vis absorption spectra of high M_n C12DPP-π-BT:PCBM (weight ratio 1:2) (purple), low M_n C12DPP-π-BT:PCBM (weight ratio 1:2) (pink), high M_n C12DPP-π-BT:P3HT (weight ratio 1:1) (orange), and low M_n C12DPP-π-BT:P3HT (weight ratio 1:1) (green) in thin films. (c) Photoluminescence of pristine high M_n C12DPP-π-BT thin film (red) is completely quenched in the presence of PCBM shown by the photoluminescence from high M_n C12DPP-π-BT:PCBM (weight ratio 1:2) thin film (purple). (d) Photoluminescence of pristine P3HT thin film (blue) is partially quenched in the presence of C12DPP-π-BT (red) shown by the photoluminescence from high M_n C12DPP-π-BT:P3HT (weight ratio 1:1) thin film (orange).

extensively studied system P3HT:PCBM with built-in potential of 0.7−1.3 eV (calculated from the reported ranges for the HOMO level of P3HT and the LUMO level of PCBM),[24,41,42] C12DPP-π-BT exhibits a larger built-in potential (1.6 eV) whether blended to form an acceptor with P3HT or blended to form a donor with PCBM (Table 1, Figure 1e,f). This suggests that photoinduced excitons would be separated effectively at the interface between C12DPP-π-BT and either P3HT or PCBM.[41,43]

3.3. Optical Properties. The UV/Vis absorption spectra for both the low M_n and high M_n C12DPP-π-BT, shown in Figure 2a,b, indicate the maximum absorptions are at 580 nm. After mixing with PCBM, the peak absorption showed a reproducible blue shift to 568 nm for the low M_n C12DPP-π-BT, whereas the high M_n C12DPP-π-BT mixture remained at the same peak position as in the pure C12DPP-π-BT film. The slight shift observed for the low M_n C12DPP-π-BT:PCBM mixture may arise from disordering of the semicrystalline structure caused by blending the polymer with PCBM, as shown in x-ray diffraction studies in Figure S1 in the Supporting Information.[6,44] The absorption spectra of the C12DPP-π-BT:P3HT mixtures showed very similar resonances for both high and low M_n C12DPP-π-BT at 550 nm.

PL quenching was used as a measure of donor−acceptor photoinduced charge transfer between the combinations of (1) C12DPP-π-BT and PCBM and (2) C12DPP-π-BT and P3HT.[45] In Figure 2c, the PL spectra of the high M_n C12DPP-π-BT film and a blend of C12DPP-π-BT and PCBM showed that the PL of C12DPP-π-BT is completely quenched when mixed with PCBM, indicating effective charge transfer between the two components. In contrast, in Figure 2d, the PL spectra of P3HT and the C12DPP-π-BT:P3HT blended films show only partial quenching of the PL of P3HT or C12DPP-π-BT. In this mixture, the P3HT emission overlaps with the C12DPP-π-BT absorption in the spectral range of 600 nm to 700 nm. This spectral overlap may give rise to possible energy transfer between the two materials. In this case, upon illumination, the excitation energy may be transferred from the exciton donor (in this case, P3HT) to the exciton acceptor (C12DPP-π-BT), which would decrease the luminescence of P3HT, and enhance the luminescence of C12DPP-π-BT (Figure 2d). Possible energy transfer from P3HT to C12DPP-π-BT provides a potentially competing pathway to charge separation in the polymer−polymer blend.[46] In comparison, faster rates of energy transfer (~1 ps) than charge transfer (~10s of ps) are reported in the literature for polymer−polymer blends and are believed to be limited by larger donor−acceptor intermolecular distance introduced by the solubilizing, long, alkyl side chains, that more dramatically affect charge rather than energy transfer.[47] Charge transfer rates are reported to be considerably faster (<ps) in polymer-PCBM blends as the small size of PCBM is anticipated to allow for closer approach to the main polymer chain.[47,48]

3.4. Optimizing C12DPP-π-BT:PCBM Blend Inter-mixing Using an Additive. The control over mixing of the different components in the blended films is crucial for bulk heterojunction solar cell fabrication.[49] To effectively separate charge carriers, it is very important to structure the semiconductor to have a large area donor−acceptor interface spaced by distances less than the exciton diffusion length, typically 5−20 nm[50] for organic semiconductors. Several strategies have been used in other reports to structure a favorable interpenetrated network, including: thermal annealing, chemical modification of the donor materials, and the use of additives to improve the miscibility of different components.[51] To improve C12DPP-π-BT:PCBM miscibility and prevent large-scale phase separation, we added a small amount (5 wt %) of diiodooctane to the C12DPP-π-BT and PCBM mixture solution. Bulk heterojunction solar cells were fabricated and optimized with the device structure of ITO/PEDOT:PSS/C12DPP-π-BT:PCBM/LiF/Al, where PEDOT:PSS serves as a hole extraction layer, whereas LiF lowers the work function of Al and serves as an electron extraction layer.[52] An overall device efficiency increase of 150% has been observed, with a 38% increase in short circuit current (I_{sc}), 19% increase of V_{oc} and 53% increase of fill factor (FF), comparing with the devices without the diiodooctane additive (see Figure S2 in the Supporting Information). To further understand the effects of the additive and to quantify the uniformity of our devices, spatially resolved photoconductivity was used to map the I_{sc} of solar cells through the transparent ITO back contact. For comparison, the recorded I_{sc} was normalized to the maximum current in each device with the high current regions indicated by bright yellow and low current regions by black. As shown in Figure 3, for C12DPP-π-BT:PCBM devices, across the entire examined area (10 μm by 10 μm), the photocurrent maps obtained for devices (a) without any additive shows non-uniformities, whereas maps for devices (b) with the diiodooctane additive are significantly more uniform, consistent with a more homogeneous blend. The histogram of the spatially resolved photocurrents (a) for C12DPP-π-BT:PCBM cells without the diiodooctane additive revealed a broad and random distribution, consistent with our conclusion of more varied performance across the device area. Photocurrent histograms for high M_n C12DPP-π-BT:PCBM devices (b) with the additive showed a narrow quasi-normal distribution peaked at 95% of the photocurrent maximum value. TEM images (shown in the Supporting Information, Figure S3) also support that high M_n C12DPP-π-BT:PCBM blends with the

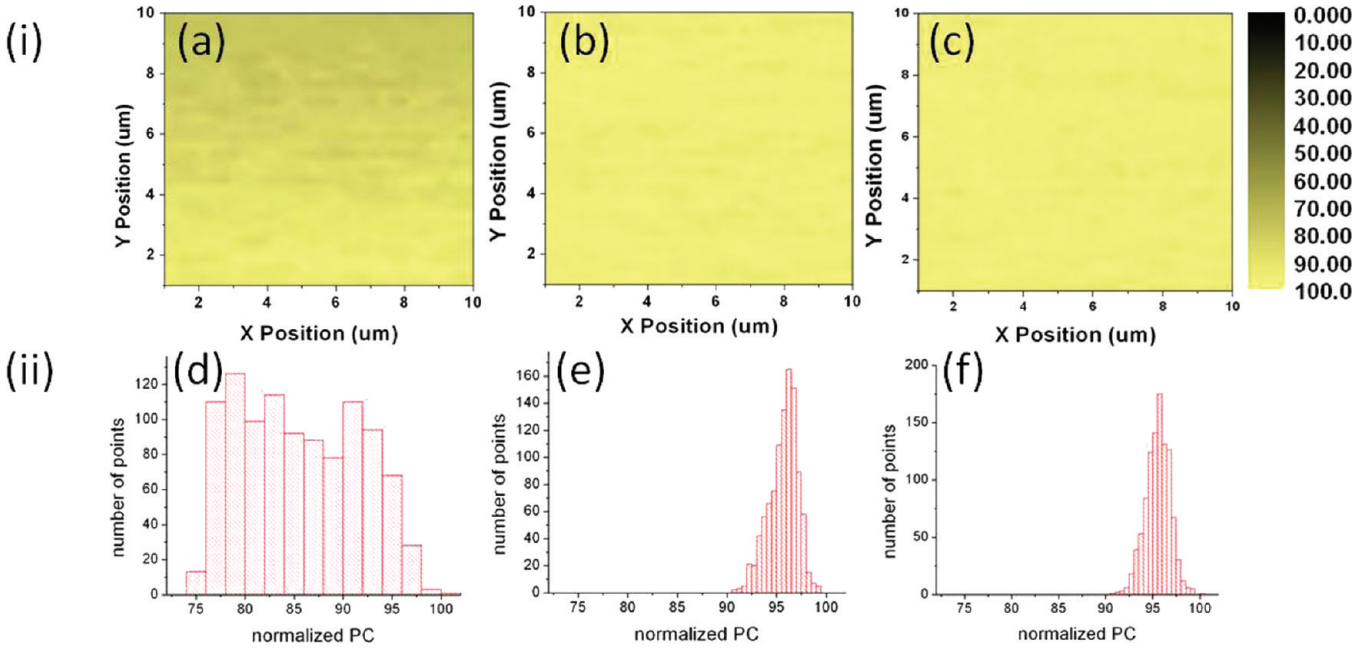

Figure 3. (i) Spatially resolved maps and (ii) histograms of short circuit current for high M_n C12DPP-π-BT:PCBM solar cells (a) without and(b) with the 5 wt % diiodooctane added to the active layer and for (c) high M_n C12DPP-π-BT:P3HT solar cells.

diiodooctane additive show much less aggregation of PCBM and hence less phase separation of C12DPP-π-BT and PCBM. All C12DPP-π-BT:P3HT devices, fabricated similarly, as shown in Figure 3(c), showed a very uniform I_{sc} without any additive, due to the good miscibility of C12DPP-π-BT and P3HT. This may be a result of the similar thiophene containing chemical structure of both polymers and their good solubility in the chloroform solvent.[53,54]

3.5. Photovoltaic Performance and Space Charge Limited Current (SCLC) Measurements. Bulk heterojunction solar cells were fabricated with the device structure of ITO/PEDOT:PSS/C12DPP-π-BT:PCBM (or C12DPP-π-BT:P3HT)/LiF/Al. Diiodooctane was added to all the C12DPP-π-BT:PCBM blends in chloroform solution for better inter-mixing. Figure 4 shows the I−V curves of the devices with the best photovoltaic performance. The devices based on the high M_n C12DPP-π-BT:PCBM demonstrated a moderate power conversion efficiency of 1.67% with I_{sc} of 7.8 mA/cm^2 and V_{oc} of 0.58 V. This is nearly a 50% improvement compared with the power conversion efficiency (1.12%) of the same polymer with a lower M_n, which had an I_{sc} of 6.4 mA/cm^2 and V_{oc} of 0.50 V, respectively. On the basis of the measurements of five different devices made under the same fabrication conditions, the average efficiency for high and low M_n polymer devices is 1.53 and 1.03%, respectively. We report and compare C12DPP-π-BT:PCBM blends with a weight ratio of 1:2 as we observed higher PCBM loadings gave better solar cell performance, consistent with higher PCBM loadings providing a more continuous pathway for electron transport.[55] The best devices based on C12DPP-π-BT:P3HT showed a moderate power conversion efficiency of 0.84% for high M_n devices with I_{sc} of 2.6 mA/cm^2 and V_{oc} of 0.92 V. Best devices with the lower M_n showed a lower efficiency of 0.73% with I_{sc} of 2.4 mA/cm^2 and V_{oc} of 0.89 V. The average efficiency for high and low M_n polymer devices is 0.76 and 0.62%, respectively, calculated for five different devices for each M_n. The statistics of device performance is summarized in Figure S4 in the Supporting Information. Further optimization using higher boiling point solvents and different processing conditions to improve the I_{sc} and FF are under investigation.

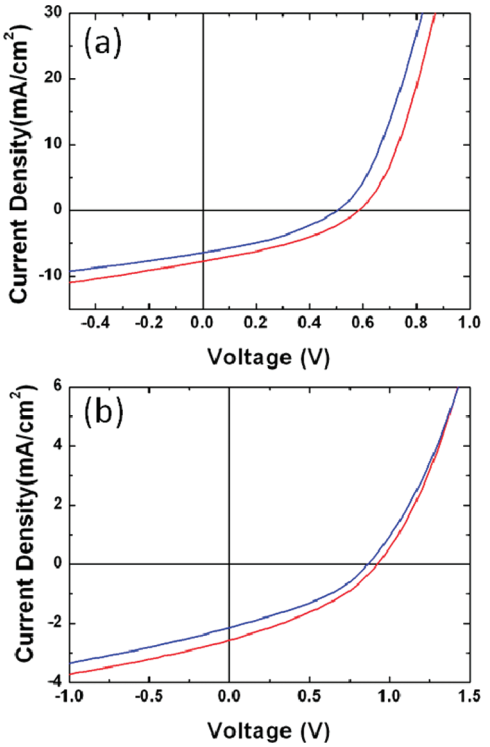

Figure 4. Current−voltage characteristics of (a) C12DPP-π-BT:PCBM (weight ratio 1:2) bulk heterojunction solar cells with high (red) and low (blue) M_n C12DPP-π-BT and (b) C12DPP-π-BT:P3HT (weight ratio 1:1) solar cells with high (red) and low (blue) M_n C12DPP-π-BT under the illumination of AM 1.5, 100 mW/cm^2.

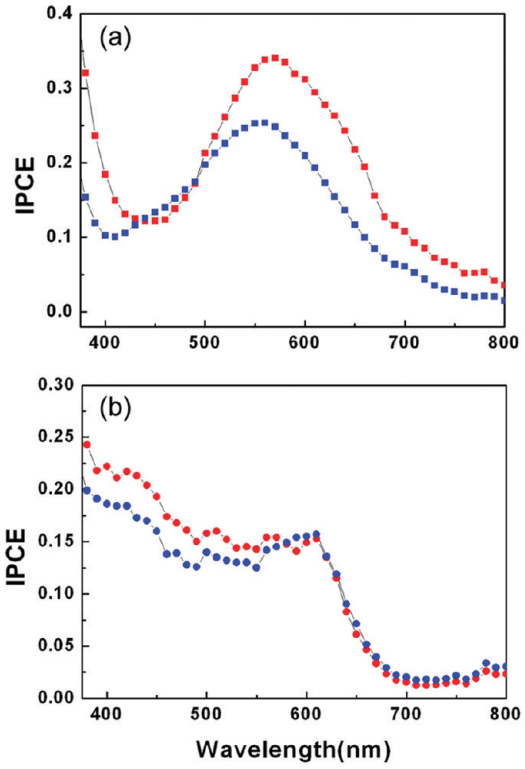

Figure 5. (a) IPCE of C12DPP-π-BT:PCBM (weight ratio 1:2) thin film solar cells for high M_n (red square) and low M_n (blue square) polymers. (b) IPCE of C12DPP-π-BT:P3HT (weight ratio 1:1) thin film solar cells for high M_n (red circle) and low M_n (blue circle) C12DPP-π-BT.

In addition to solar simulated illumination, the spectral response/incident photon conversion efficiency (IPCE) of the devices as a function of excitation energy was measured (Figure 5). The devices exhibit high external quantum efficiencies over 30% for the high M_n C12DPP-π-BT:PCBM blends. The shape of IPCE curves matches the absorption spectra of the respective blends. Similar results have been observed for diketopyrrolopyrrole-based polymer:PCBM blends spin-coated from chloroform solutions.[9] C12DPP-π-BT:P3HT devices maintain external quantum efficiency around 15% over a broad spectral range from 400 to 600 nm, which indicates the high-energy spectral components contribute more significantly to the IPCE. We hypothesize the difference between IPCE and absorption spectra arises from the increase in recombination as the excitation intensity increases at longer wavelengths and/or the two polymers contribute differently to the photocurrent.

C12DPP-π-BT can function as either an electron donor when mixed with PCBM or an electron acceptor when blended with P3HT. To further confirm the ambipolar transport properties of C12DPP-π-BT, the hole and electron mobilities of the polymer were characterized by the space charge limited current (SCLC) model, which is a commonly used tool by checking the space charge limited current through the semiconductor in the dark in a sandwich structure.[56,57] To investigate hole transport through the device, high work function electrodes ITO/PEDOT:PSS and palladium (Pd) were used. These electrodes form barriers to electron injection of 1.7 eV with C12DPP-π-BT. In contrast, for the electron mobility analysis, Al and LiF/Al were used as hole-blocking contacts with a hole injection barrier of 1.2 eV between polymer and the Al contact and 1.9 eV between polymer and the LiF/Al contact. The current-voltage data are shown in Figure S5 in the Supporting Information, fitted to the following equation[58,59]

$$J_{e(h)} = \left(\frac{9}{8}\right)\varepsilon\varepsilon_0\mu_{0e(h)}\exp\left(0.891\gamma_{e(h)}\sqrt{\frac{V}{d}}\right)V^2/d^3 \qquad (1)$$

where $\mu_{0e(h)}$ is the zero-field electron/hole mobility, $\gamma_{0e(h)}$ is the field activation factor, V is the applied potential and d is the thickness of the active layer. $\mu_{0e(h)}$ and $\gamma_{0e(h)}$ were evaluated by fitting the current−voltage characteristics. At room temperature, a zero-field hole mobility of 2.1x10^{-4} cm^2/(V s) and electron mobility of 4.7 $\times$ 10^{-5} cm^2/(V s) were obtained for the high M_n C12DPP-π-BT only device. Similarly, a zero-field hole mobility of 4.2 $\times$ 10^{-5} cm^2/(V s) and electron mobility of 2.5 $\times$ 10^{-5} cm^2/(V s) were obtained for the low M_n polymer only device. This indicates good charge transport for both electrons and holes. As a comparison, P3HT showed a hole mobility of 2.2 $\times$ 10^{-5} cm^2/(V s), which is consistent with the literature reported value of 3 $\times$ 10^{-5} cm^2/(V s).[60] SCLC measurements in the diode configuration commonly yield significantly lower carrier mobilities than field-effect mobility measurements in the transistor configuration. We have fabricated and characterized top-contact, bottom-gate transistors having C12DPP-π-BT semiconducting channels with field-effect hole mobilities of 0.04 $\pm$ 0.004 cm^2/(V s) for high M_n polymer and 0.03 $\pm$ 0.005 cm^2/(V s) for low M_n polymer, showing a slightly better transport for the higher M_n polymer, consistent with the SCLC results and better OPV performance (see Figure S6 in the Supporting Information).

For C12DPP-π-BT:PCBM devices and C12DPP-π-BT:P3HT devices, the higher M_n polymer displayed higher efficiency originating from both higher V_{oc} and higher I_{sc} than the lower M_n polymer, consistent with greater photogeneration (in C12DPP-π-BT:PCBM devices) and carrier transport in the higher M_n blends. From the absorption spectra of the mixed film, shown in Figure 2b, the higher M_n C12DPP-π-BT:PCBM has a larger absorption coefficient than the low M_n C12DPP-π-BT:PCBM mixture, and unlike the low M_n C12DPP-π-BT:PCBM mixture, the higher M_n C12DPP-π-BT:PCBM absorbs further to the red, showing no blue shift in absorption upon blending. The higher and more extended red absorption of the higher M_n C12DPP-π-BT:PCBM blend is reflected in a ~9% higher peak IPCE efficiency and the IPCE spectrum extends further to the red. SCLC measurements revealed higher hole and electron mobilities for the high M_n polymer compared to the low M_n polymer. The morphology of the blended films was also investigated by atomic force microscopy (AFM) (Figure 6). The morphology and phase images suggest that the higher M_n polymer forms larger grains in either blends with PCBM or blends with P3HT, reducing the number of grain boundaries that may trap charges, and hence provides more facile pathways for carrier transport.[29]

It is also interesting to point out that the C12DPP-π-BT:P3HT devices showed much higher V_{oc} than C12DPP-π-BT:PCBM devices, even though the built-in potentials calculated from electrochemical measurements are the same (1.6 eV) for both configurations. However, in practice, the obtainable V_{oc} is always lower than the upper limit value derived from isolated materials characteristics and thermodynamic considerations, because of electrode-active layer and donor−acceptor interfacial energetics and non-radiative recombination losses.

(1) To maximize V_{oc} for heterojunction solar cells, Ohmic contacts are generally required, imposing energy level

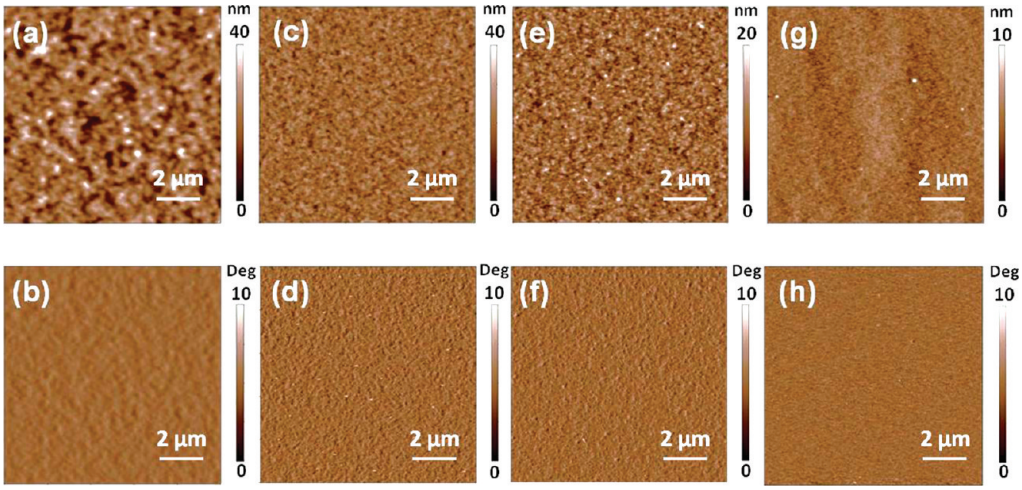

Figure 6. AFM topography and phase images of (a, b) high M_n C12DPP-π-BT:PCBM (weight ratio 1:2), (c, d) low M_n C12DPP-π-BT:PCBM (weight ratio 1:2), (e, f) high M_n C12DPP-π-BT:P3HT (weight ratio 1:1), and (g, h) low M_n C12DPP-π-BT:P3HT (weight ratio 1:1) with scan range (10 by 10 μm). All samples were annealed at 140 °C for 20 min.

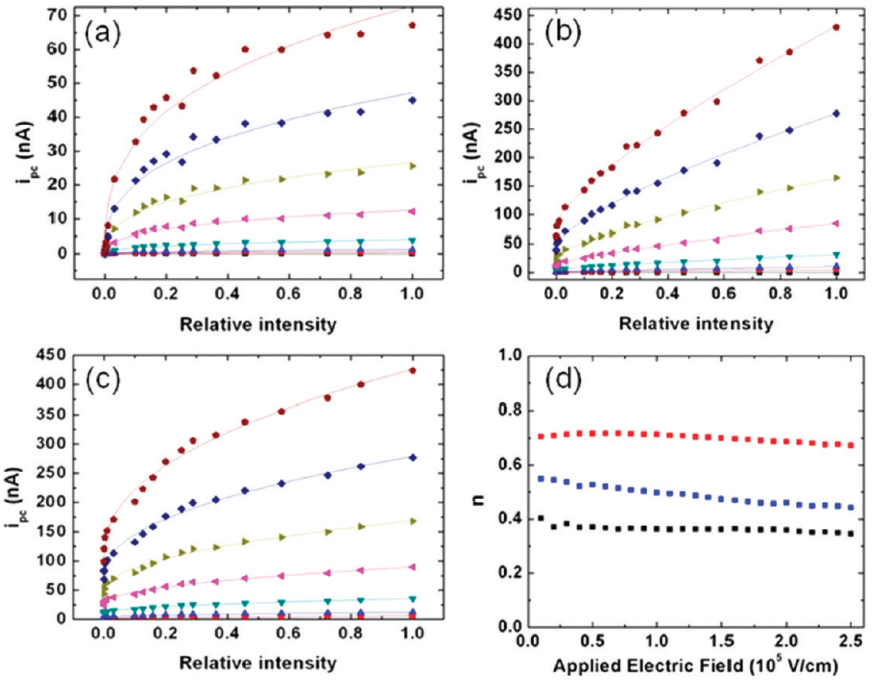

Figure 7. Intensity dependence of the photocurrent for (a) high M_n C12DPP-π-BT only thin films, (b) high M_n C12DPP-π-BT:PCBM blend thin films, and (c) high M_n C12DPP-π-BT:P3HT blend thin films at applied electric fields of (black square) 0, (red circle) 0.1, (blue triangle) 0.2, (green triangle) 0.5, (pink triangle) 1.0, (olive green triangle) 1.5, (blue diamond) 2.0, and (brown circle) 2.5×10^5 V/cm. (d) Power values, n, of the function $i_{pc} \propto I_0^n$ vs electric field for (black square) the high M_n C12DPP-π-BT only, (red square) the high M_n C12DPP-π-BT:PCBM blend, and (blue square) high M_n C12DPP-π-BT:P3HT blend. Laser: 488 nm, 19.8 A, 0.291 W. Intensity at the sample: 16.6 W/cm^2 for the largest intensity (relative intensity = 1).

alignment of the HOMO level of the electron donor with the Fermi level of the hole collecting PEDOT:PSS/ITO electrode and of the LUMO level of the electron acceptor with the Fermi level of the electron collecting LiF/Al electrode.[61] A thin layer of LiF reduces the work function of Al from 4.2 to 3.5 eV,[39] aligning it with the LUMO levels for both PCBM and C12DPP-π-BT and forming Ohmic contacts. The PEDOT:PSS electrode has a work function of 5.1 $\pm$ 0.2 eV.[62] The contact effects will limit the V_{oc} if the donor polymer has a HOMO level more negative than −5.3 eV versus vacuum,[61] which is consistent with a lower V_{oc} for C12DPP-π-BT:PCBM devices. For the C12DPP-π-BT:P3HT system, the donor polymer P3HT has a HOMO level around −5.1 eV, which makes the PEDOT:PSS electrode a suitable Ohmic contact to maximize the V_{oc}.

(2) Different interfacial dipoles may exist at the C12DPP-π-BT:PCBM and C12DPP-π-BT:P3HT interfaces, which can alter the effective Coulombic binding energy of the exciton and therefore affect the V_{oc} of solar cells.[63]

(3) In addition, according to Shockley and Queisser's paper, the maximum thermodynamic V_{oc} value can only be reached in the absence of non-radiative recombination.[64] To better understand charge generation and recombination process in these systems and hence their effects on device performance, we characterized the light intensity dependence of photoconductivity. Figure 7 shows the photocurrent versus relative intensity of 2.43 eV (488 nm) excitation at different electric fields for (a) high M_n C12DPP-π-BT, (b) high M_n C12DPP-π-BT:PCBM blends, and (c) high M_n C12DPP-π-BT:P3HT blends films. Fitting the curves to $i_{pc} \propto I_0^n$, the exponent n for the pure polymer sample was ~0.4, indicating a bimolecular nature of recombination that has a square-root dependence on intensity. For C12DPP-π-BT:P3HT devices, the exponent n remains at ~0.5; this is characteristic of bimolecular recombination, indicating the absence of deep traps in the film. In contrast, after blending with PCBM, the mixed sample showed an increase in n to ~0.7. This reveals the existence of both bimolecular recombination and monomolecular recombination, a competing process that has a linear dependence on excitation intensity. The first-order recombination kinetics suggest the presence of more recombination centers in the C12DPP-π-BT:PCBM mixture than in pure C12DPP-π-BT and in the C12DPP-π-BT:P3HT mixture, such as charge carrier traps at the interface of the two materials.[65] Trap-assisted recombination is consistent with the V_{oc} measured in C12DPP-π-BT:PCBM devices being lower than the value deduced from the difference between acceptor LUMO and donor HOMO.[66] In addition, the existence of charge traps can increase the recombination of electrons and holes thereby reducing the fill factor, which is an important limitation on device efficiency.[65,67]

CONCLUSION

In conclusion, we report the synthesis, characterization, and implementation of a new diketopyrrolopyrrole-based polymer with energy levels located between those of commonly used electron donor and electron acceptor materials. Unlike previously reported diketopyrrolopyrolle-based polymers and small molecules, which have only been used as either the electron donor or acceptor in OPVs, we show that C12DPP-π-BT can function as either an electron donor or electron acceptor in solution-processable organic photovoltaics. A moderate power conversion efficiency of 1.67% was achieved with the high M_n C12DPP-π-BT polymer: PCBM blend devices and 0.84% with higher M_n C12DPP-π-BT polymer:P3HT blend devices. SCLC measurements confirm both electron and hole transport in the C12DPP-π-BT copolymer. We demonstrate higher M_n polymer gives rise to increased photon generation and carrier transport and therefore higher I_{sc}, V_{oc}, and overall OPV efficiency. Comparing C12DPP-π-BT:PCBM and C12DPP-π-BT:P3HT devices, which are characterized by the same built-in potential from electrochemical calculations, a higher I_{sc}, but smaller V_{oc} is obtained for C12DPP-π-BT:PCBM devices. The higher I_{sc} in C12DPP-π-BT:PCBM devices is believed to originate from ultrafast, efficient charge transfer and more balanced electron and hole transport, whereas the V_{oc} is limited by trap-assisted recombination and interfacial contact losses. In contrast, the C12DPP-π-BT:P3HT system achieves higher V_{oc}, yet suffers from lower I_{sc} because of the possible limitation in charge transfer hindered by long alkyl chain, which will increase the intramolecular distance and prevent the closer contact of two polymers. The rational design of donor−acceptor copolymers provides organic photovoltaic materials with large built-in potentials and balanced electron and hole transport, promising efficient OPVs. Further optimization of materials design and processing, such as shorter, yet solubilizing, branched side chains and investigation of solvents and annealing effects[9] to increase charge transfer in polymer−polymer blends and improve morphologies to reduce carrier trapping in polymer-PCBM blends, are being pursued to increase device efficiencies. Finally, the strong photoluminescence and ambipolar nature of C12DPP-π-BT make it a promising candidate for organic light-emitting diode and organic light emitting transistor applications.

ASSOCIATED CONTENT

Supporting Information. Details of general characterization methods, XRD charaterization and discussion, I−V and TEM characterization of devices without diiodooctane addtives, statistics of OPV devices performace, FET fabrication and characterization, and SCLC simulation (PDF). This material is available free of charge via the Internet at http://pubs.acs.org.

AUTHOR INFORMATION

Corresponding Author

*Tel: 1-215-573-4384. Fax: 1-215-573-2068. E-mail: kagan@seas.upenn.edu.

ACKNOWLEDGMENT

This work was supported by the American Chemical Society Petroleum Research Foundation (PRF-49260-ND10) and the National Science Foundation CBET program (CBET-0854226).

REFERENCES

(1) Bijleveld, J. C.; Zoombelt, A. P.; Mathijssen, S. G. J.; Wienk, M. M.; Turbiez, M.; de Leeuw, D. M.; Janssen, R. A. J. *J. Am. Chem. Soc.* **2009**, *131*, 16616.

(2) Günes, S.; Neugebauer, H.; Sariciftci, N. S. *Chem. Rev.* **2007**, *107*, 1324.

(3) Hou, J.; Chen, H.-Y.; Zhang, S.; Chen, R. I.; Yang, Y.; Wu, Y.; Li, G. *J. Am. Chem. Soc.* **2009**, *131*, 15586.

(4) Park, S. H.; Roy, A.; Beaupre, S.; Cho, S.; Coates, N.; Moon, J. S.; Moses, D.; Leclerc, M.; Lee, K.; Heeger, A. J. *Nat. Photonics* **2009**, *3*, 297.

(5) Walker, B.; Tamayo, A. B.; Dang, X.-D.; Zalar, P.; Seo, J. H.; Garcia, A.; Tantiwiwat, M.; Nguyen, T.-Q. *Adv. Funct. Mater.* **2009**, *19*, 3063.

(6) Li, G.; Shrotriya, V.; Huang, J.; Yao, Y.; Moriarty, T.; Emery, K.; Yang, Y. *Nat. Mater.* **2005**, *4*, 864.

(7) Yu, C.-Y.; Chen, C.-P.; Chan, S.-H.; Hwang, G.-W.; Ting, C. *Chem. Mater.* **2009**, *21* (14), 3262.

(8) Peng, Q.; Park, K.; Lin, T.; Durstock, M.; Dai, L. *J.Phys. Chem. B* **2008**, *112* (10), 2801.

(9) Wienk, M. M.; Turbiez, M.; Gilot, J.; Janssen, R. A. J. *Adv. Mater.* **2008**, *20* (13), 2556.

(10) Chen, L.; Deng, D.; Nan, Y.; Shi, M.; Chan, P. K. L.; Chen, H. *J.Phys. Chem. C* **2011**, *115* (22), 11282.

(11) Shi, M.-M.; Deng, D.; Chen, L.; Ling, J.; Fu, L.; Hu, X.-L.; Chen, H.-Z. *J. Polym. Sci., Part A: Polym. Chem.* **2011**, *49* (6), 1453.

(12) Sun, S. S., Sariciftci, N. S. *Organic Photovoltaics*; CRC Press: Boca Raton, FL, 2005.

(13) Chan, W. K.; Chen, Y.; Peng, Z.; Yu, L. *J. Am. Chem. Soc.* **1993**, *115* (25), 11735.
(14) Bao, Z.; Chan, W. K.; Yu, L. *J. Am. Chem. Soc.* **1995**, *117* (50), 12426.
(15) Behnke, M.; Tieke, B. *Langmuir* **2002**, *18* (10), 3815.
(16) Beyerlein, T.; Tieke, B.; Forero-Lenger, S.; Brütting, W. *Synth. Met.* **2002**, *130* (2), 115.
(17) Zhu, Y.; Zhang, K.; Tieke, B. *Macromol. Chem. Phys.* **2009**, *210* (6), 431.
(18) Zhou, E.; Yamakawa, S.; Tajima, K.; Yang, C.; Hashimoto, K. *Chem. Mater.* **2009**, *21* (17), 4055.
(19) Karsten, B. P.; Bijleveld, J. C.; Janssen, R. A. J. *Macromol. Rapid Commun.* **2010**, *31*, 1554.
(20) de Leeuw, D. M.; Simenon, M. M. J.; Brown, A. R.; Einerhand, R. E. F. *Synth. Met.* **1997**, *87*, 53.
(21) Huo, L.; Hou, J.; Chen, H.-Y.; Zhang, S.; Jiang, Y.; Chen, T. L.; Yang, Y. *Macromolecules* **2009**, *42*, 6564.
(22) Li, Y.; Singh, S. P.; Sonar, P. *Adv. Mater.* **2010**, *22*, 4862.
(23) Zhou, E.; Wei, Q.; Yamakawa, S.; Zhang, Y.; Tajima, K.; Yang, C.; Hashimoto, K. *Macromolecules* **2009**, *43*, 821.
(24) Li, Y.; Sonar, P.; Singh, S. P.; Soh, M. S.; van Meurs, M.; Tan, J. *J. Am. Chem. Soc.* **2011**, *133*, 2198.
(25) Coulson, D. R.; Satek, L. C.; Grim, S. O. *Inorg. Syn.* **1972**, *13*, 121.
(26) Kozma, E.; Kotowski, D.; Bertini, F.; Luzzati, S.; Catellani, M. *Polymer* **2010**, *51*, 2264.
(27) Murphy, A. R.; Liu, J.; Luscombe, C.; Kavulak, D.; Fréchet, J. M. J.; Kline, R. J.; McGehee, M. D. *Chem. Mater.* **2005**, *17*, 4892.
(28) Rabindranath, A. R.; Zhu, Y.; Heim, I.; Tieke, B. *Macromolecules* **2006**, *39*, 8250.
(29) Wu, M.-C.; Lo, H.-H.; Liao, H.-C.; Chen, S.; Lin, Y.-Y.; Yen, W.-C.; Zeng, T.-W.; Chen, Y.-F.; Chen, C.-W.; Su, W.-F. *Sol. Energy Mater. Sol. Cells* **2009**, *93*, 869.
(30) Brabec, C. J.; Cravino, A.; Meissner, D.; Sariciftci, N. S.; Fromherz, T.; Rispens, M. T.; Sanchez, L.; Hummelen, J. C. *Adv. Funct. Mater.* **2001**, *11*, 374.
(31) Gregg, B. A. *J.Phys. Chem. B* **2003**, *107*, 4688.
(32) Moliton, A.; Nunzi, J.-M. *Polym. Int.* **2006**, *55*, 583.
(33) Pommerehne, J.; Vestweber, H.; Guss, W.; Mahrt, R. F.; Bässler, H.; Porsch, M.; Daub, J. *Adv. Mater.* **1995**, *7*, 551.
(34) Cardona, C. M.; Li, W.; Kaifer, A. E.; Stockdale, D.; Bazan, G. C. *Adv. Mater.* **2011**, *23*, 2367.
(35) Brabec, C., Dyakonov, V., Scherf, U. *Organic Photovoltaics: Materials, Device Physics, and Manufacturing Technologies*; Wiley-VCH: New York, 2008.
(36) Lof, R. W.; van Veenendaal, M. A.; Koopmans, B.; Jonkman, H. T.; Sawatzky, G. A. *Phys. Rev. Lett.* **1992**, *68*, 3924.
(37) Veldman, D.; Meskers, S. C. J.; Janssen, R. A. J. *Adv. Funct. Mater.* **2009**, *19* (12), 1939.
(38) Park, Y.; Choong, V.; Gao, Y.; Hsieh, B. R.; Tang, C. W. *Appl. Phys. Lett.* **1996**, *68*, 2699.
(39) Eremina, N.; Degtyarenko, K.; Kopylova, T.; Samsonova, L.; Gadirov, R.; Maier, G. *Theor. Exp. Chem.* **2009**, *45*, 63.
(40) Tengstedt, C.; Kanciurzewska, A.; de Jong, M. P.; Braun, S.; Salaneck, W. R.; Fahlman, M. *Thin Solid Films* **2006**, *515*, 2085.
(41) Scharber, M. C.; Mühlbacher, D.; Koppe, M.; Denk, P.; Waldauf, C.; Heeger, A. J.; Brabec, C. J. *Adv. Mater.* **2006**, *18*, 789.
(42) Davis, R. J.; Lloyd, M. T.; Ferreira, S. R.; Bruzek, M. J.; Watkins, S. E.; Lindell, L.; Sehati, P.; Fahlman, M.; Anthony, J. E.; Hsu, J. W. P. *J. Mater. Chem.* **2011**, *21*, 1721.
(43) Rand, B. P.; Burk, D. P.; Forrest, S. R. *Phys. Rev. B* **2007**, *75*, 115327.
(44) Aernouts, T. V., P.; Haeldermans, I.; D'Haen, J.; Heremans, P.; Poortmans, J.; Manca, J. V. *Mater. Res. Soc. Symp. Proc.* **2007**, 1013.
(45) Sariciftci, N. S.; Smilowitz, L.; Heeger, A. J.; Wudl, F. *Science* **1992**, *258*, 1474.
(46) Koeppe, R.; Fuchsbauer, A.; Lu, S.; Sariciftci, N. S *Progr Colloid Polym Sci* **2008**, *135*, 16.
(47) Hideo, O.; Junya, K.; Jiamo, G.; Hiroaki, B.; Shinzaburo, I. *J. Photon. Energy* **2011**, *1*, 011118.
(48) Bakulin, A. A.; Hummelen, J. C.; Pshenichnikov, M. S.; van Loosdrecht, P. H. M. *Adv. Funct. Mater.* **2010**, *20*, 1653.
(49) Chen, L.-M.; Hong, Z.; Li, G.; Yang, Y. *Adv. Mater.* **2009**, *21*, 1434.
(50) Gur, I.; Fromer, N. A.; Chen, C.-P.; Kanaras, A. G.; Alivisatos, A. P. *Nano Lett.* **2006**, *7*, 409.
(51) Peet, J.; Senatore, M. L.; Heeger, A. J.; Bazan, G. C. *Adv. Mater.* **2009**, *21*, 1521.
(52) Chen, L.-M.; Xu, Z.; Hong, Z.; Yang, Y. *J. Mater. Chem.* **2010**, *20* (13), 2575.
(53) Gedde, U. W. *Polymer Physics*; Kluwer Academic Publishers: Dordrecht, The Netherlands, 1995.
(54) Krause, S. *Pure Appl. Chem.* **1986**, *58*, 1553.
(55) Mihailetchi, V. D.; Koster, L. J. A.; Blom, P. W. M.; Melzer, C.; de Boer, B.; van Duren, J. K. J.; Janssen, R. A. J. *Adv. Funct. Mater.* **2005**, *15*, 795.
(56) Bozano, L.; Carter, S. A.; Scott, J. C.; Malliaras, G. G.; Brock, P. J. *Appl. Phys. Lett.* **1999**, *74*, 1132.
(57) Melzer, C.; Koop, E. J.; Mihailetchi, V. D.; Blom, P. W. M. *Adv. Funct. Mater.* **2004**, *14* (9), 865.
(58) Murgatroyd, P. N. *J. Phys. D: Appl. Phys.* **1970**, *3*, 151.
(59) Matsushima, T.; Murata, H. *Appl. Phys. Lett.* **2009**, *95*, 203306.
(60) Chiguvare, Z.; Dyakonov, V. *Phys. Rev. B* **2004**, *70*, 235207.
(61) Bijleveld, J. C.; Verstrijden, R. A. M.; Wienk, M. M.; Janssen, R. A. J. *Appl. Phys. Lett.* **2010**, *97*, 073304.
(62) Tengstedt, C.; Crispin, A.; Hsu, C. H.; Zhang, C.; Parker, I. D.; Salaneck, W. R.; Fahlman, M. *Org. Electron.* **2005**, *6*, 21.
(63) Pensack, R. D.; Banyas, K. M.; Barbour, L. W.; Hegadorn, M.; Asbury, J. B. *Phys. Chem. Chem. Phys.* **2009**, *11*, 2575.
(64) Shockley, W.; Queisser, H. J. *J. Appl. Phys.* **1961**, *32*, 510.
(65) Morana, M.; Wegscheider, M.; Bonanni, A.; Kopidakis, N.; Shaheen, S.; Scharber, M.; Zhu, Z.; Waller, D.; Gaudiana, R.; Brabec, C. *Adv. Funct. Mater.* **2008**, *18*, 1757.
(66) Mandoc, M. M.; Kooistra, F. B.; Hummelen, J. C.; Boer, B. d.; Blom, P. W. M. *Appl. Phys. Lett.* **2007**, *91*, 263505.
(67) Hau, S. K.; Yip, H.-L.; Acton, O.; Baek, N. S.; Ma, H.; Jen, A. K. Y. *J. Mater. Chem.* **2008**, *18*, 5113.